A new interface element connecting 3D finite elements with non-coincident nodes to simulate delamination in composite laminates

Antoine Trellu, Christophe Bouvet, Samuel Rivallant, Léon Ratsifandrihana

▶ **To cite this version:**

Antoine Trellu, Christophe Bouvet, Samuel Rivallant, Léon Ratsifandrihana. A new interface element connecting 3D finite elements with non-coincident nodes to simulate delamination in composite laminates. Composite Structures, 2020, 252, pp.112694. 10.1016/j.compstruct.2020.112694 . hal-02954039

HAL Id: hal-02954039
https://hal.science/hal-02954039

Submitted on 30 Sep 2020

HAL is a multi-disciplinary open access archive for the deposit and dissemination of scientific research documents, whether they are published or not. The documents may come from teaching and research institutions in France or abroad, or from public or private research centers.

L'archive ouverte pluridisciplinaire **HAL**, est destinée au dépôt et à la diffusion de documents scientifiques de niveau recherche, publiés ou non, émanant des établissements d'enseignement et de recherche français ou étrangers, des laboratoires publics ou privés.

Open Archive Toulouse Archive Ouverte (OATAO)

OATAO is an open access repository that collects the work of some Toulouse researchers and makes it freely available over the web where possible.

This is an author's version published in: https://oatao.univ-toulouse.fr/26734

Official URL: https://doi.org/10.1016/j.compstruct.2020.112694

To cite this version :

Trellu, antoine and Bouvet, Christophe and Rivallant, Samuel and Ratsifandrihana, Léon A new interface element connecting 3D finite elements with non-coincident nodes to simulate delamination in composite laminates. (2020) Composite Structures, 252. ISSN 0263-8223

Any correspondence concerning this service should be sent to the repository administrator:
tech-oatao@listes-diff.inp-toulouse.fr

A new interface element connecting 3D finite elements with non-coincident nodes to simulate delamination in composite laminates

A. Trellu [a,b], C. Bouvet [a,*], S. Rivallant [a], L. Ratsifandrihana [b]

[a] Université de Toulouse, Institut Clément Ader, ISAE-SUPAERO – UPS – IMT Mines Albi – INSA, 10 av. E. Belin, 31055 Toulouse, France
[b] SEGULA Aerospace and Defence, 24 bd. Déodat de Severac, 31770 Colomiers, France

Keywords:
Delamination
Crack propagation
Interface element
Numerical modeling

A B S T R A C T

Composite failure phenomena remain complex and lead to over-size structures in many industries, involving long and costly experimental campaigns. Numerical approaches are a good alternative to decrease sizing costs. The Discrete Ply Model developed in Institut Clément Ader over these last ten years shows good results in simulation of impact and compression after impact of composite laminates, ply drop-offs, open hole tensile tests… But the present approach leads to certain limitations for complex stacking sequences and induces unwanted characteristic lengths between consecutive plies. A user element for delamination calculation is developed that allows to define an interface corresponding to the overlapping zone between the two volume elements of upper and lower plies, whereas this overlapping zone is not directly defined by nodes of the mesh (volume elements have non-coincident nodes). The present paper details the new interface element implementation, its validation from DCB and ENF test simulations, and then its improvement is discussed.

1. Introduction

Composites structures made of unidirectional plies are more and more used in the aeronautical industry because of their high strength-to-weight ratio. However, their vulnerability to out-of-plane loading, such as low velocity impacts, leads to an over-sizing. These loadings can appear during ground operations when aircraft parts are exposed to unexpected impacts as tool drops [1]. Composite failure phenomena remain complex and analytical models proposed in the literature [2,3] are too limited to design composite structures and to take into account interactions between the main damage mechanisms (fiber failure, matrix cracking and delamination) [4]. Moreover, testing new structures involves long and costly experimental campaigns. Thus, there is a real need to turn to virtual testing approach [5] to address this issue and to get a better understanding of composite behavior. Since the 90's, many researches deal with numerical finite element modelling to simulate damage involved by low velocity impact on composite laminates [2,6,7]. This is the case of the "Discrete Ply Model" (DPM) developed by Bouvet et al. for over ten years [8–12], which shows good results in simulation of impact and compression after impact of composite laminates, ply drop-offs, open hole tensile tests… The DPM is implemented in the commercial finite element solver Abaqus/Explicit with a user subroutine VUMAT which describes the main damage mechanisms developing in a composite structure, i.e. matrix cracking, delamination and fiber failure.

The principle of the DPM is to use one volume element in the thickness of each unidirectional ply of the laminate, and to represent both transverse matrix cracking and delamination between plies with interface elements (Fig. 1), matrix cracking interface elements being parallel to the fiber orientation. In the current version of the DPM, the use of standard cohesive elements available in Abaqus [13] to represent delamination imposes coincidence of nodes between neighboring plies, which leads to the specific mesh presented in Fig. 1, structured by the fiber orientation of each ply. This mesh philosophy, also used in [14–16], gives a good localization of matrix cracking, and allows to naturally account for the coupling between matrix cracking and delamination. It has been proved that this coupling is essential in order to well simulate the damage developing during an impact test and in particular is very important to get a good orientation of the delamination propagation of the lower ply [17–20].

Unfortunately, there are a number of limitations due to this meshing concept. The first one is a pure geometrical problem: only standard ply orientations (0°, 90° and ±45°) can be used in the current model, due to the need for a coincident mesh between plies. The second limitation is the impossibility to have different volume element widths in different plies. It is an important point since element length and width

* Corresponding author.
E-mail address: christophe.bouvet@isae.fr (C. Bouvet).

https://doi.org/10.1016/j.compstruct.2020.112694

Nomenclature

DPM	Discrete Ply Model
DCB	Double Cantilever Beam
ENF	End Notched Flexure
VUMAT	user material subroutine in Abaqus
VUEL	user element subroutine in Abaqus
VCCT	Virtual Crack Closure Technique
CZM	Cohesive Zone Model
P_i	Virtual interface nodes
$P_i^{'}$	Virtual interface nodes with bending curvature improvement
k_i	Virtual interface spring stiffness
λ_i	Distance ratio to link displacement of virtual and real interface nodes
$\underline{\underline{\pi}}$	Linear function matrix linking virtual and real nodes
$\underline{\underline{K}}$	Linear function matrix linking virtual and real nodes
U_i	Real node displacements vector
U_{Pi}	Virtual node displacements vector
F_i	Real node forces vector
F_{Pi}	Real node forces vector
d_{eq}	Equivalent displacement for the cohesive law
d_i	Displacement jump (I: out-of-plane, II & III: in plane)
d_i^0	Critical displacement jump (I: out-of-plane, II & III: in plane)
G_{ic}	Delamination critical energy release rate (I: out-of-plane, II & III: in plane)
Δ	Opening displacement in DCB test
a_0	Initial crack length
a	Crack length
u	Specimen deflection in ENF test

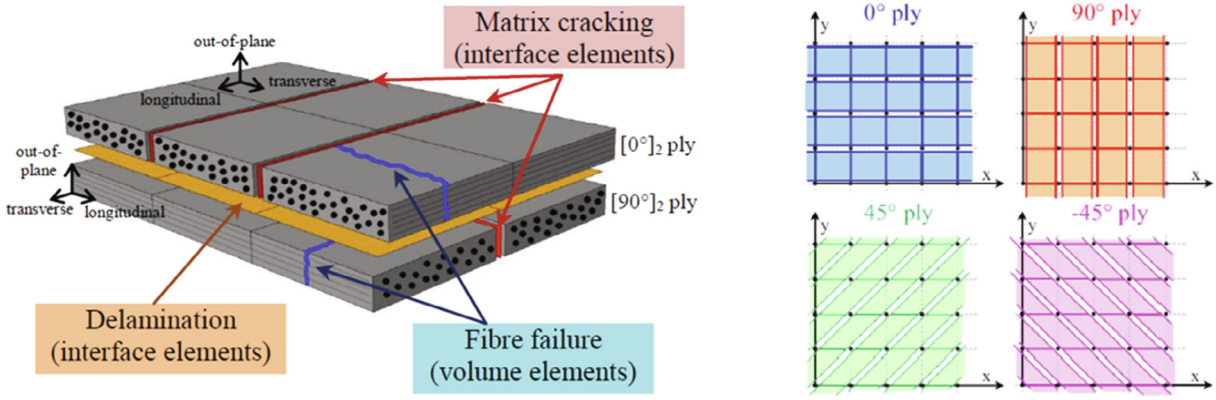

Fig. 1. DPM concept and imposed mesh (Rivallant et al. [10]).

are linked in the DPM even if these two characteristic lengths are physically independent. Indeed element width is dependent on the ply thickness because the distance between two consecutive intralaminar cracks is linked to the ply thickness. For example, Maimi et al. [21] showed that the transverse stress failure is dependent on the ply thickness and Leopold et al. [22] showed that the distance between two matrix cracks in a ply ranges from one to three times the ply thickness (Fig. 2). Then to respect this length between two consecutive cracks, the distance between two consecutive cohesive elements for matrix cracking should be ranged between one and three times the ply thickness. In the case of laminates made of different kinds of plies with different thicknesses, or in the case of stacking with contiguous plies in the same orientation, constraints on the distance between cracks imposes different widths in the volume element, a priori incompatible with the current mesh. The third limitation is a matter of computation time, also important for a use in the industry. As the volume element length in the fiber direction is only linked to the fiber failure, it could be reasonably increased (independently of width) to reduce the global number of elements and degrees of freedom in the model, and thus CPU time. Indeed, in the DPM, fiber failure is taken into account by dissipating the fracture toughness independently of the element length [23].

To sum up, with the purpose to improve the DPM and broaden the domain of application, it is necessary to find an alternative to standard interface elements for delamination in order to represent plies in whatever direction and to be able to modify volume element length and width in two consecutive plies, independently each of other. This

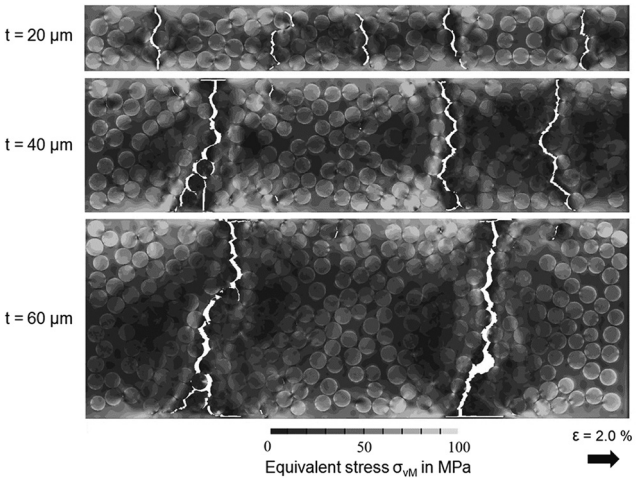

Fig. 2. 90° ply thickness influence (20, 40 and 60 µm) on the distance between matrix cracks for an imposed deformation of 2% (Leopold et al. [22]).

should be done for plies with non-coincident nodes. Of course, the field of applications of such an interface element is not reduced only to out-of-plane impact. It can be of interest in various cases concerning composite delamination in large structures and complex laminates. Finally, it is also important that this alternative can be implemented in a commercial software to be accessible to industrial engineers.

The most common ways to simulate delamination in composite structures are models based on the Virtual Crack Closure Technique (VCCT) [24] and the Cohesive Zone Model (CZM). For technical reasons linked to the fact that the DPM is implemented in the commercial software Abaqus/Explicit, the VCCT approach is not explored in this study. The CZM, introduced by [25] and [26], uses cohesive interface elements located between plies. This method is widely used for low velocity impact models [14,16,27–30] and is the current solution used in the DPM to simulate delamination and matrix cracking. One of the main issues in the formulation of interface elements in the CZM approach for complex models is the need for kinematic compatibility between interface elements and their neighboring elements. First developments [31–33] were done for delamination between usual linear or quadratic volume elements (or equivalent in 2D), with zero or non-zero thickness elements that led to the standard interface elements available in most of finite element software. Usually, a traction-separation law is associated to these elements. Various cohesive laws are proposed in the literature. Most common are bilinear [34], polynomial, trapezoidal [35] and exponential traction-separation laws. To model precisely crack propagation phenomena these cohesive laws can be coupled or improved. Jensen et al. [36] used classic delamination elements with a mixed-mode multilinear law with 15 different segments to study delamination R-curve effects on glass composite laminate.

For more complex problems, it can be necessary to enrich the interface elements itself to adapt them to their neighboring elements. In Davila et al. [37], to model laminates as a stacking of shells and interface elements (one shell per ply, one interface element between two plies), a non-zero thickness 8-node cohesive element is developed to link nodes of the shells taking into account the rotational degrees of freedom at the shell nodes and the gap between the shells. In the same philosophy, to represent fracture damage in reinforced concrete beams, Kohnehpooshi et al. [38] proposed a specific interface element between 20-node isoparametric solid Brick elements and plate bending elements representing respectively the concrete and the composite plate reinforcement. More recently, Navarro et al. [39] developed a new damageable shell-to-shell 8-node interface element. Contrary to Davila et al. [37], they chose to represent the real resin interface between plies with a non-zero thickness, which led them to introduce virtual nodes at the out-of-plane position of the real resin interface, connected to real shell nodes with rigid elements. One can also mention works done on volume elements that are prone to delaminate and then split into two shell elements to represent delaminated plies [40,41], but it does not answer the question of non-coincident nodes.

To the author's knowledge, many works deal with the enrichment of cohesive laws or the improvement of the element itself, but in each of these cases the interface element building is based on node coincidence between the two crack face and node to face sticking. Nevertheless this last method does not look suitable for the present problem and the aim to decrease computation time.

One can also cite remeshing methods, meshless methods [42], or more recent developed moving mesh methods [43]. They can all be of great interest, but are more complex to implement, especially in a commercial software.

Thus, this paper presents the development of a new zero-thickness interface element to simulate delamination between layers of volume elements without coincident nodes. This element is developed as a user-defined element so that it can be implemented in a commercial finite element software and used in an industrial setting. Abaqus/Explicit was chosen for this study, using a VUEL subroutine to define the user-element. The element formulation is based on virtual nodes, located at the vertex of the overlapping zone between the two volume elements of upper and lower plies. From these eight virtual nodes, a standard element is defined inside the user element. No new physical nodes are added to the model: the user element nodes are nodes from the neighboring volume elements. Damage law implemented in the interface element is not discussed here, as it is the same as the one used in the current version of the DPM. In order to evaluate the efficiency of this new interface element, delamination tests in mode I and mode II were simulated. The mode I is obtained with a "Double Cantilever Beam" test (DCB) [44], the mode II with an "End Notched Flexure" test (ENF) [45].

First, the formulation of the new interface element is explained in Section 2. Section 3 presents the first results obtained with the new interface. An improvement of the user element is then described in Section 4 and associated results are presented in Section 5. Finally, conclusions of this work are given in Section 6.

2. New interface element formulation

Fig. 3 shows an example of two-ply laminate mesh achievable with the new interface element. Compared to the previous mesh (Fig. 1), nodes of the upper and lower plies are no more coincident. This non-coincidence makes it possible to increase the element size in the fiber orientation and to use different element widths in two consecutive plies. The interface element is reduced to the overlapping zone between two volume elements. To represent the plies, C3D8I volume elements with incompatible modes are used in order to improve the bending behavior even with one element in the ply thickness [46]. This work only focuses on 8-node interface elements corresponding to the four-sides overlapping zones colored in green in Fig. 3, but can be generalized to the other unclassical cases. Fig. 4 presents in details the 8-node interface element between two volume elements with different fiber orientations.

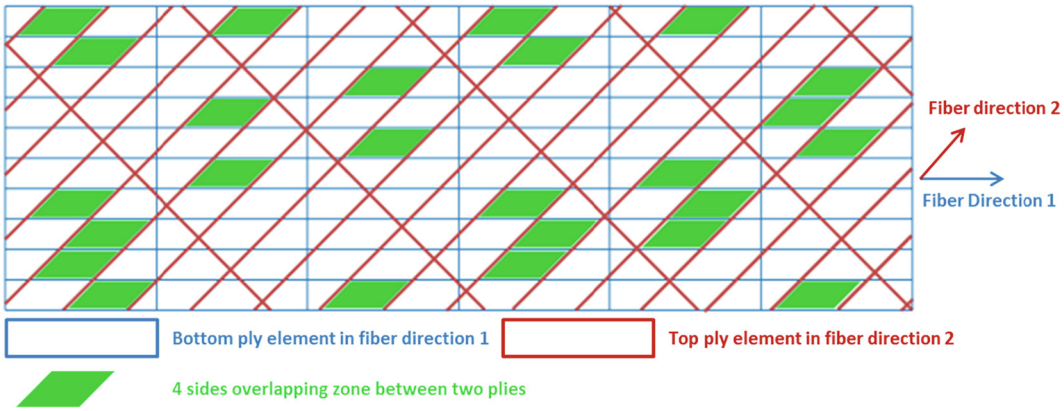

Fig. 3. Mesh possibilities with the new interface element.

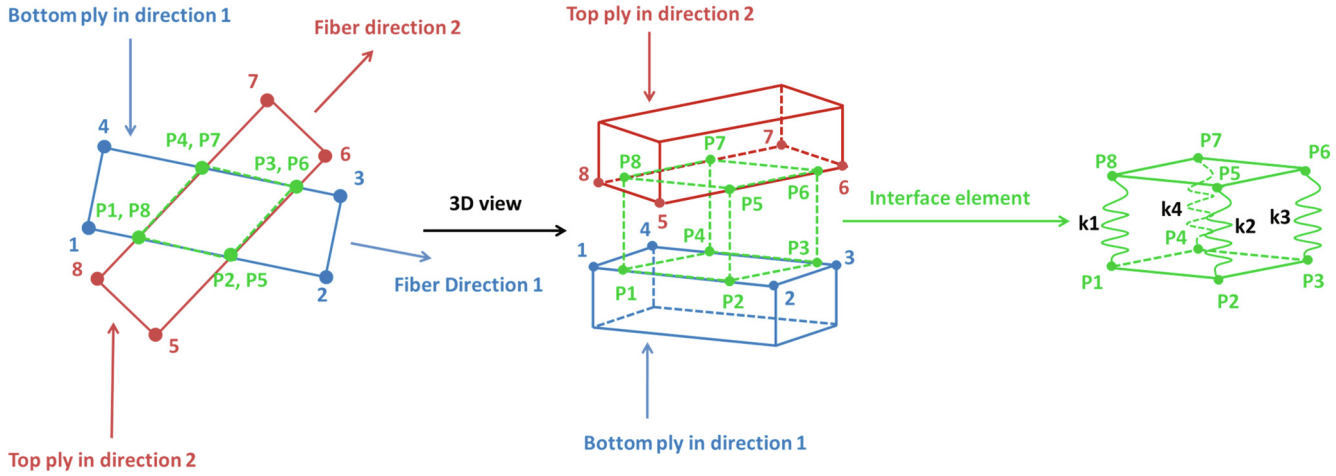

Fig. 4. New interface element.

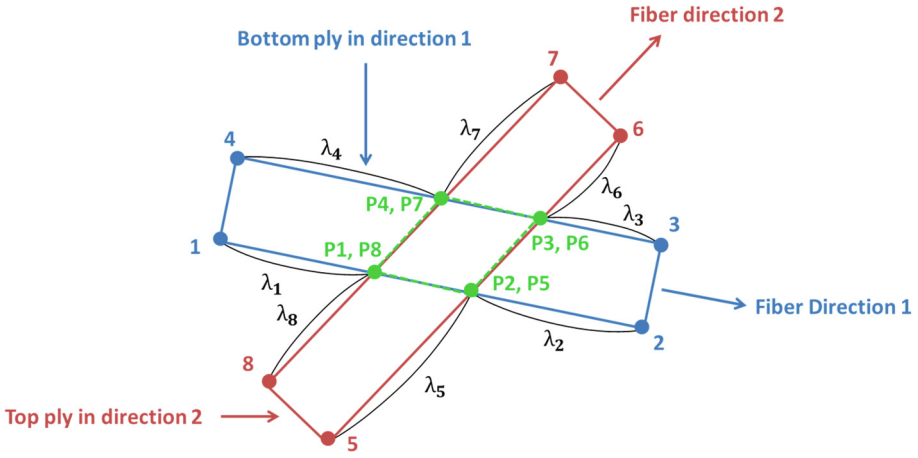

Fig. 5. Distance ratios λ_1 to.λ_8

The 8-node user element is defined in Abaqus/Explicit in a VUEL subroutine. The eight nodes are the four upper nodes of the bottom ply element (1, 2, 3 and 4 in blue) and the four lower nodes of the top ply element (5, 6, 7 and 8 in red). But as the interface considered for delamination calculation is only the overlapping zone, eight virtual nodes are defined at element edges intersections: P_1 to P_8 (in green). This interface is shown in three dimensions in the figure for a better understanding, but at the initial state, it is a zero-thickness element. In fact, from these eight virtual nodes, a classical cohesive zone element can be defined with twelve springs: three springs of equal stiffness for each couple of upper and lower virtual nodes (one in the out-of-plane direction z, and two in the laminate plane axes x and y). Only springs in the out-of-plane direction are depicted in Fig. 4. Spring stiffnesses for each couple of nodes are k_1, k_2, k_3 and k_4.

Thus, this new interface element is like a classical interface element embedded in a wider user element. After adding a traction-separation law, the interface behavior is fully defined inside the user element. Finally, the main issue regarding the development of this element is the calculation of load transfer between the volume element nodes (1 to 8) and the interface virtual nodes (P_1 to P_8), taking account of eventual failure propagation in the element.

Displacements at nodes P_1 to P_8 are determined according to displacements of the volume elements nodes through a shape function matrix. This matrix is composed of the distance ratios λ_1 to λ_8 which are calculated from the initial geometry (Fig. 5).

Eqs. (1) and (2) give displacement calculation for nodes P_1 to P_8 according to volume elements nodes displacements U_{x1} to U_{x8} and the shape function matrix $\underline{\underline{\pi}}$. Matrix $\underline{\underline{\pi}}$ represents the linear functions linking displacement of virtual nodes P_1 to P_4 with displacement of nodes 1–4 and displacement of virtual nodes P_5 to P_8 with displacement of nodes 5 to 8 in the global axes. For simplicity, equations are given only for x direction, but they are the same for y and z directions.

$$\begin{bmatrix} U_{xP1} \\ \vdots \\ U_{xP8} \end{bmatrix} = \underline{\underline{\pi}} \begin{bmatrix} U_{x1} \\ \vdots \\ U_{x8} \end{bmatrix} \tag{1}$$

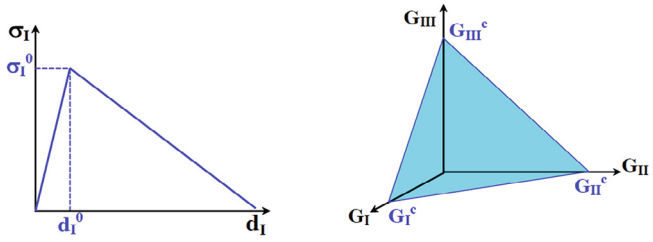

Fig. 6. Delamination law in mode I and delamination modes coupling (Bouvet et al. [9]).

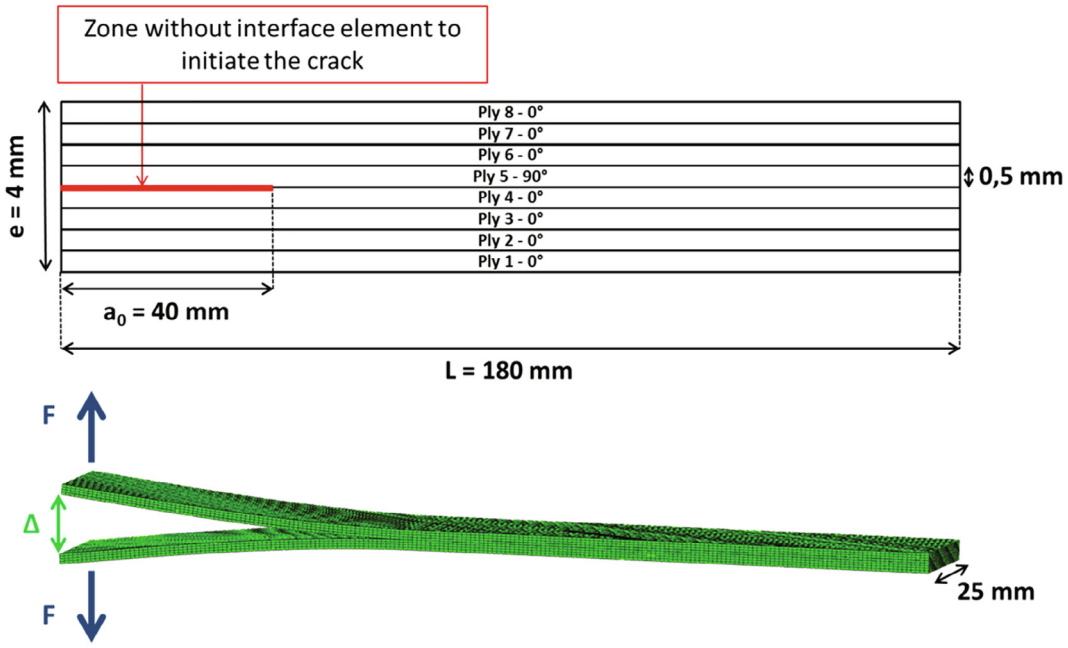

Fig. 7. DCB specimen.

$$\underline{\underline{\pi}} = \begin{pmatrix} 1-\lambda_1 & \lambda_1 & 0 & 0 & 0 & 0 & 0 & 0 \\ \lambda_2 & 1-\lambda_2 & 0 & 0 & 0 & 0 & 0 & 0 \\ 0 & 0 & 1-\lambda_3 & \lambda_3 & 0 & 0 & 0 & 0 \\ 0 & 0 & \lambda_4 & 1-\lambda_4 & 0 & 0 & 0 & 0 \\ 0 & 0 & 0 & 0 & 1-\lambda_5 & \lambda_5 & 0 & 0 \\ 0 & 0 & 0 & 0 & \lambda_6 & 1-\lambda_6 & 0 & 0 \\ 0 & 0 & 0 & 0 & 0 & 0 & 1-\lambda_7 & \lambda_7 \\ 0 & 0 & 0 & 0 & 0 & 0 & \lambda_8 & 1-\lambda_8 \end{pmatrix} \tag{2}$$

The element stiffness matrix $\underline{\underline{K}}$ is calculated with the four spring stiffness coefficients and allows to determine forces at nodes P_1 to P_8 according to the displacements U_{P1} to U_{P8} (Eqs. (3) and (4)). In fact, this calculation step and the following damage calculation are run in the interface local coordinate frame.

$$\begin{bmatrix} F_{xP1} \\ \vdots \\ F_{xP8} \end{bmatrix} = \underline{\underline{K}} \begin{bmatrix} U_{xP1} \\ \vdots \\ U_{xP8} \end{bmatrix} \tag{3}$$

$$\underline{\underline{K}} = \begin{pmatrix} k1 & 0 & 0 & 0 & 0 & 0 & 0 & -k1 \\ 0 & k2 & 0 & 0 & -k2 & 0 & 0 & 0 \\ 0 & 0 & k3 & 0 & 0 & -k3 & 0 & 0 \\ 0 & 0 & 0 & k4 & 0 & 0 & -k4 & 0 \\ -k1 & 0 & 0 & 0 & 0 & 0 & 0 & k1 \\ 0 & -k2 & 0 & 0 & k2 & 0 & 0 & 0 \\ 0 & 0 & -k3 & 0 & 0 & k3 & 0 & 0 \\ 0 & 0 & 0 & -k4 & 0 & 0 & k4 & 0 \end{pmatrix} \tag{4}$$

Then the interface damage is driven using fracture mechanics calculated with an equivalent displacement d_{eq} for each couple of virtual nodes (Eq. (5)), as it would be in a classical cohesive zone interface element [9].

$$d_{eq} = \sqrt{\left(\langle d_I \rangle^+\right)^2 + \left(\frac{d_I^0}{d_{II}^0} d_{II}\right)^2 + \left(\frac{d_I^0}{d_{III}^0} d_{III}\right)^2} \tag{5}$$

where d_I^0, d_{II}^0 and d_{III}^0 are the critical displacements for damage initiation, respectively in fracture mode I, II and III. The displacement jump d_I, d_{II} and d_{III} are calculated from the displacements of the virtual nodes P_i respectively in out-of-plane and in-plane directions. This equivalent displacement allows to directly compare displacements in mode I, II and III, with the mode I. When the equivalent displacement d_{eq} reaches the initiation failure displacement in mode I, d_I^0, in one of the springs, stiffness of the considered spring is decreased until the good energy release rate is dissipated (Fig. 6). Moreover, to avoid penetration between plies in compression, the degradation in mode I is managed by using a non-degraded spring stiffness in compression.

Thus, forces at nodes P_1 to P_8 of the interface element can be calculated from the displacements of nodes 1 to 8 with Eq. (6):

$$\begin{bmatrix} F_{xP1} \\ \vdots \\ F_{xP8} \end{bmatrix} = \underline{\underline{K}}\,\underline{\underline{\pi}} \begin{bmatrix} U_{x1} \\ \vdots \\ U_{x8} \end{bmatrix} \tag{6}$$

And forces at volume element nodes 1 to 8 are obtained from the forces at interface virtual nodes using the transposed shape functions matrix $\underline{\underline{\pi}}^t$ [47] (Eq. (7)):

$$\begin{bmatrix} F_{x1} \\ \vdots \\ F_{x8} \end{bmatrix} = \underline{\underline{\pi}}^t \begin{bmatrix} F_{xP1} \\ \vdots \\ F_{xP8} \end{bmatrix} \tag{7}$$

3. First results in fracture mode I

As introduced in Section 1, a “Double Cantilever Beam” (DCB) test simulation is performed in order to validate the new interface element in fracture mode I. The stacking sequence is $[0^\circ_4/90^\circ/0^\circ_3]$ (the red colored line in the stacking sequence indicates the initially delaminated interface) and the ply thickness is 0.5 mm. In the model, the crack is initiated with a 40 mm long zone without interface elements. Fig. 7 shows test characteristics and specimen dimensions. The specimen width is 25 mm, F is the force and Δ is the respective opening.

Table 1 gives T700/M21 properties, the material used to run simulations. In order to get a symmetric test and to easily compare it with analytical results, the Young's modulus in the fiber direction and the transverse Young's modulus are supposed equal (even if it is physically unrealistic). In this way, the DCB test allows loading of a 0°/90° interface while the bending stiffness of specimen parts over and under the initially delaminated interface are the same. For this work fiber failure and matrix cracking are not introduced in the model, only the delamination is studied.

As said before, volume elements are meshed with C3D8I element because of their good bending behavior. Several numerical simulations were launched (Fig. 8). Indeed different configurations of the DCB test with user interface elements are simulated by changing volume element length in the fiber direction and keeping the same distance between two matrix cracking interfaces (i.e. the width of the volume elements). This is a key point to model composite laminates under impact: the final objective is to increase the length to width ratio by five in order to reduce calculation time. Issues regarding computation time for each case will be discussed in Section 5.3. Validation of these different cases is based on analytical/numerical comparisons of force/displacement curves (Fig. 9-a), crack length/displacement curves (Fig. 9-b) and fracture toughness/crack length curves (Fig. 9-c). Analytical results are obtained with the analysis method given by the fracture mode I test standard [44] and detailed in [48].

Results in Fig. 9 show that for a ratio length to width $\frac{L}{l} \leq 2$, the mode I behavior is well represented. For a ratio $\frac{L}{l} > 2$, the global behavior of the interface is coherent as shown in Fig. 9-a with force/displacement curves even if the delamination onset and the load during the propagation phase are overestimated. This overestimation results from a delay in the crack propagation (Fig. 9-b) inducing a too high value of G_{IC} (Fig. 9-c). In order to validate this new interface element for different cases, the same DCB test is perform on a thin laminate of 2 mm thickness (Fig. 10). Specimen characteristics are exactly the same as those presented in Fig. 7, only the thickness is changed, which allows to increase the bending deformation of the structure and then to evaluate the efficiency of the new interface element with higher curvature.

The DCB test of the 2 mm thick laminate is also performed by varying the length to width ratio from one to five. Results in terms of force/

Table 1
T700/M21 mechanical properties used in the model.

Elastic Properties		
E_1	*Young's modulus in fiber direction*	130 GPa
E_t	*Transverse Young's modulus (artificial value)*	130 GPa
ν_{lt}	*Poisson ratio*	0.3
G_{lt}	*Shear modulus*	4.75 GPa
Delamination		
σ_t^f	*Transverse tensile strength*	60 MPa
τ_{lt}^f	*In-plane shear strength*	110 MPa
G_{Ic}^d	*Interface fracture toughness for opening mode (I)*	0.5 N/mm
G_{IIc}^d	*Interface fracture toughness for shear mode (II & III)*	1.8 N/mm

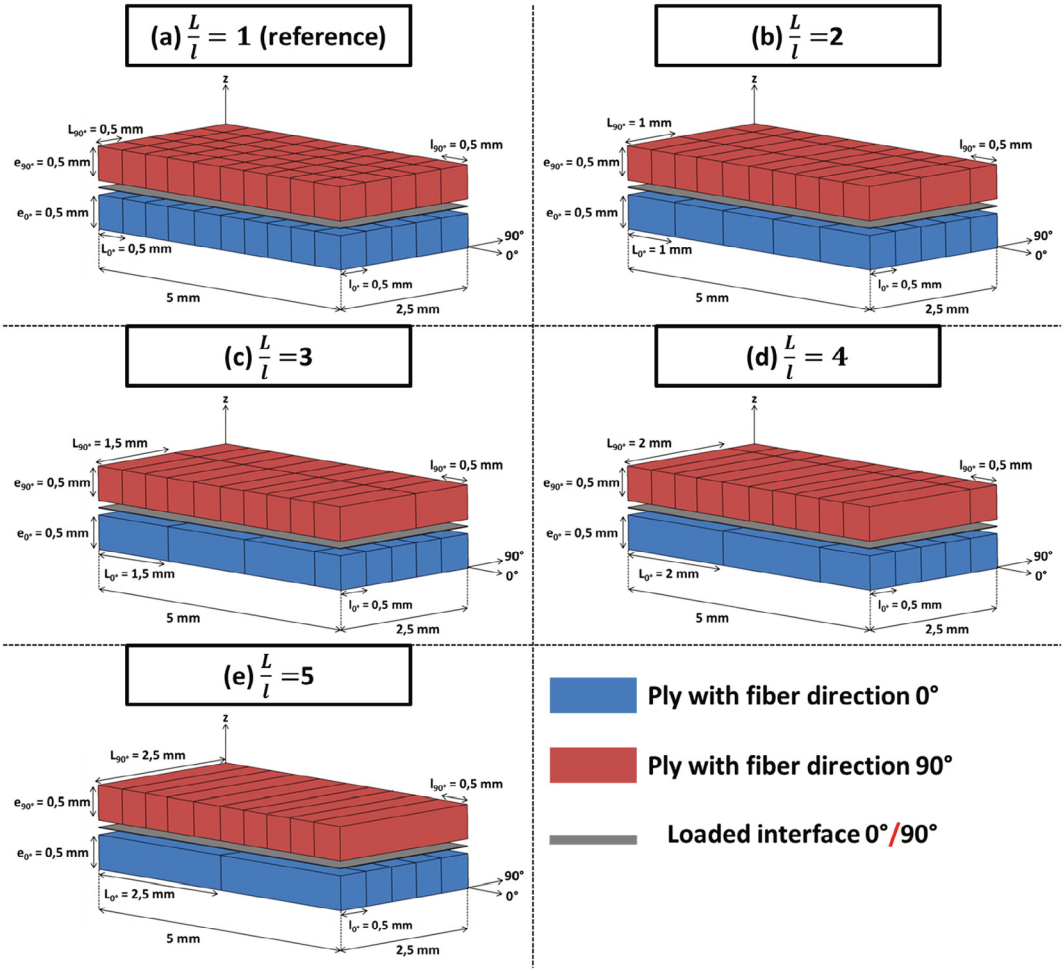

Fig. 8. Different mesh configurations tested.

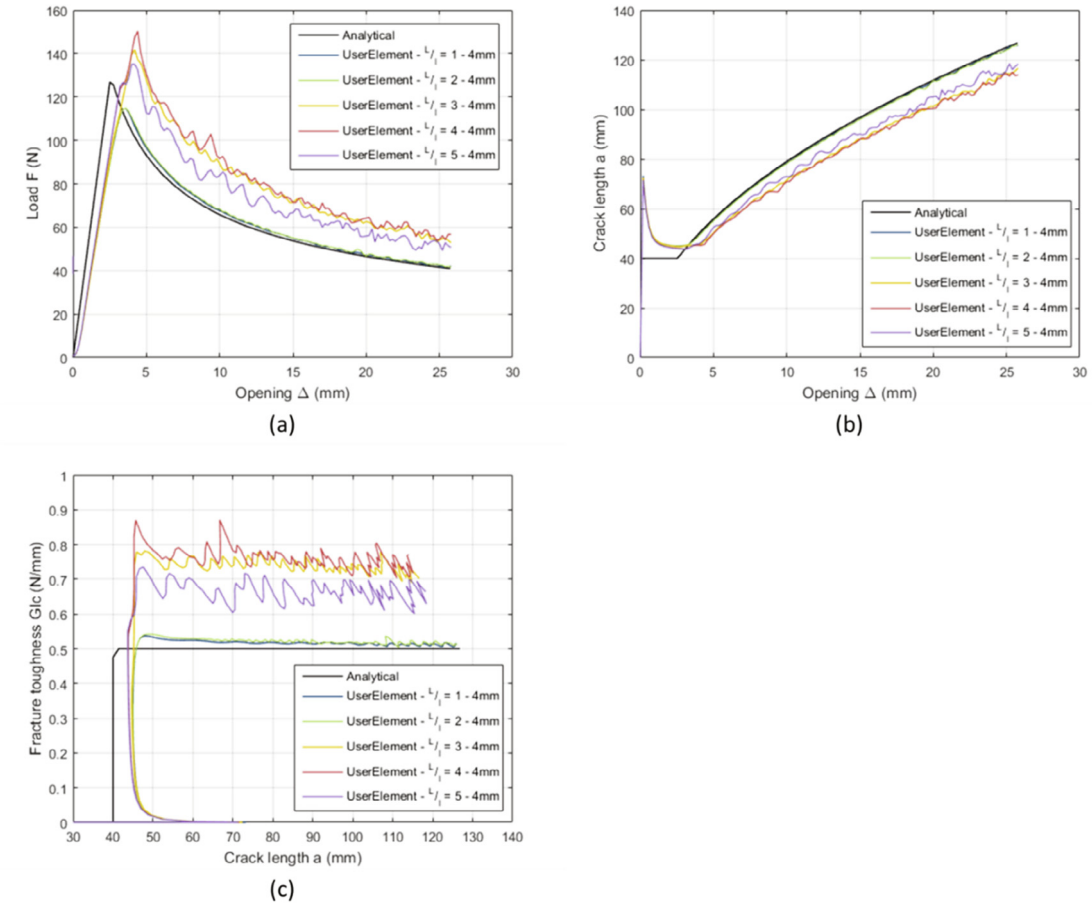

Fig. 9. Force/displacement curves (a), crack length/opening displacement curves (b) and fracture toughness/crack length curves (c) for different mesh configurations of a 4 mm thick laminate.

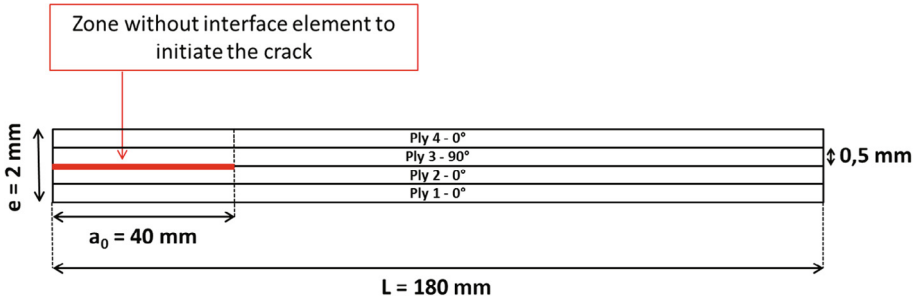

Fig. 10. Second DCB test performed with a thinner specimen of 2 mm thickness.

opening displacement curves, crack length/opening displacement curves and fracture toughness/crack length curves are given in Fig. 11.

As for the 4 mm thick laminate, the delamination is well represented until the length to width ratio exceeds 2. For $\frac{L}{l} > 2$, the error between the analytical reference load and the numerical load for the delamination onset and the propagation phase is more critical than the one observed in the thick specimen (Fig. 11-a). The error during the propagation phase is directly visible on the crack propagation. Indeed Fig. 11-b shows a delay of about 10 mm in the crack length growth for a 20 mm opening displacement. Consequently, the fracture toughness in mode I is more than twice the reference value of 0.5 N/mm (Fig. 11-c).

The delay in the crack length growth is illustrated in Fig. 12. This figure represents the deformed shape of the reference case ($\frac{L}{l} = 1$) in black and a case with longer elements ($\frac{L}{l} = 5$) in blue for a 20 mm opening displacement. This figure shows a gap of 9 mm between the reference crack length a_{ref} and the user element crack length $a_{UserElement}$. The deformed shape of the two cases is also different. For a ratio $\frac{L}{l} = 5$, the element size in the fiber direction is increased which deteriorates the finite element discretization and therefore the local bending behavior of the specimen. The delamination law being driven in displacement, the delay on the crack length growth could be explained by a poor consideration of the bending in the two arms of the 2 mm thick specimen. For the 4 mm thick laminate, the problem is less critical because the bending stiffness is more important and the curvature deformation is less pronounced. In order to fix this issue, a bending curvature consideration is implemented in the new interface element. This work is presented in the following section.

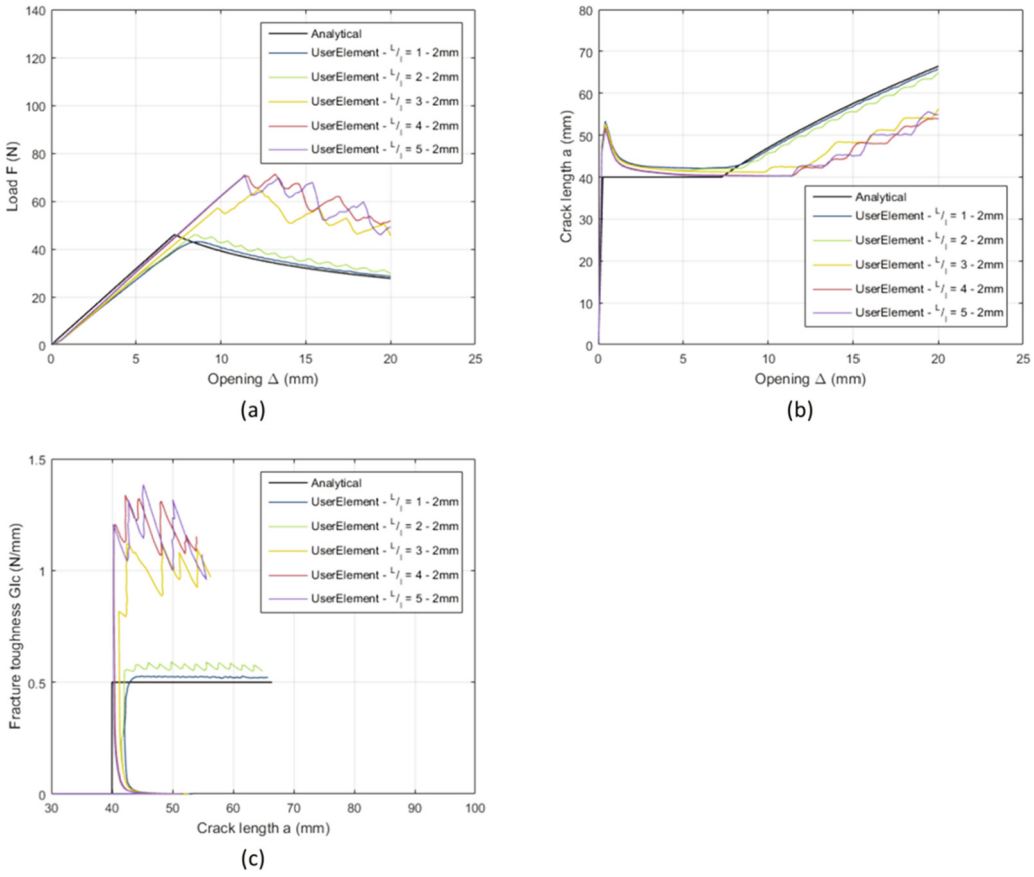

Fig. 11. Force/displacement curves (a), crack length/opening displacement curves and fracture toughness/crack length curves (c) for different mesh configurations of a 2 mm thick laminate.

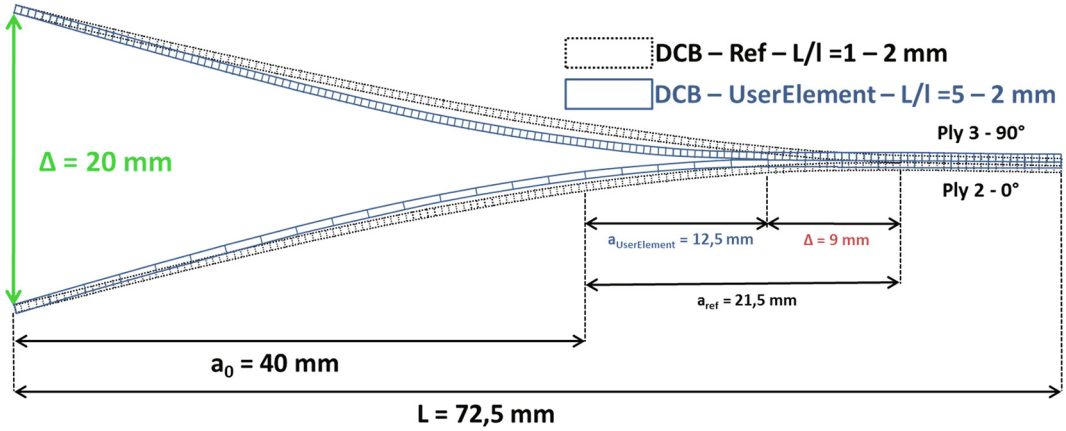

Fig. 12. Crack length growth comparison for the 2 mm thick laminate between a ratio $\frac{L}{l} = 1$ and a ratio $\frac{L}{l} = 5$ (for $\Delta = 20$ mm). Only ply 2 and ply 3 are depicted.

4. Bending curvature improvement

The objective of this part is to get a better bending curvature of the interface element by using the volume element nodes without changing volume elements formulation. The idea is to calculate the local curvature with a cubic function (Eq. (8)) to modify the position of each point P_i in the z direction (Fig. 13). It can be noticed that the cubic function is consistent with the C3D8I element shape function, which is also cubic.

$$z(x) = a_0 + b_0 x + c_0 x^2 + d_0 x^3 \tag{8}$$

To determine the constants a_0, b_0, c_0 and d_0, curvature angles θ_A and θ_B are needed. These curvature angles are not given by C3D8I elements and need to be calculated geometrically. A longer-term perspective is to replace volume elements by improved shell elements to represent fiber failure. These new shell elements would allow to directly access to curvature angles. Following points present two methods implemented and tested to calculate curvature angles.

- The first idea was to use the volume element deformed shape to calculate angles θ_1 and θ_2. To get a geometric calculation of curvature angles, a new 16-node user element was implemented including the

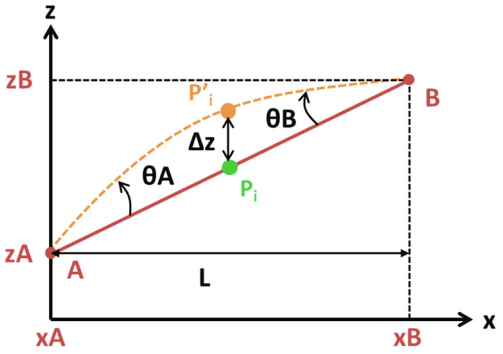

Fig. 13. Curvature calculation.

four upper nodes of the top volume element (13 to 16) and the four lower nodes of the bottom volume element (9 to 12) to have information on the whole volume elements geometry directly inside the user element (Fig. 14). Angles θ_1 and θ_2 are calculated from the right angles at nodes 1 and 2. The virtual node forces are now obtained from the new position P_1' to P_8' of the points P_1 to P_8. This method seems to be the most logical to get curvature angles with the element deformed shape, but unfortunately, it induces undesired stiffness coupling and numerical instabilities. This method should get better results with real shell elements. Indeed the C3D8I elements are not shell element but volume element with only adding incompatible modes of shear deformation [13].

- To improve the curvature estimation, it was chosen not to calculate curvature angles but to directly evaluate the new position of the point P_i (Fig. 15). The cubic function (Eq. (8)) is directly solved using the nodes coordinates in a Lagrange interpolation formula (Eq. (9)). For example, the modification of the z coordinate for vir-

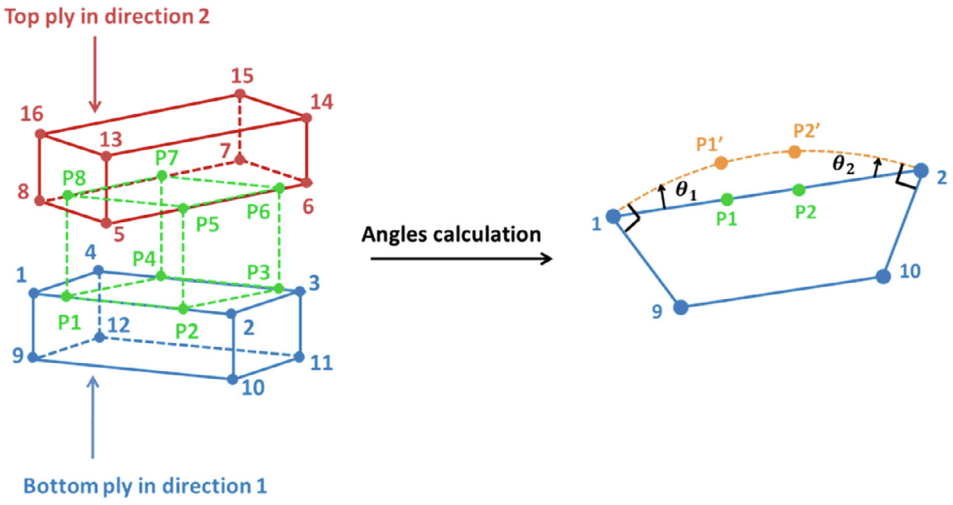

Fig. 14. First configuration for curvature calculation.

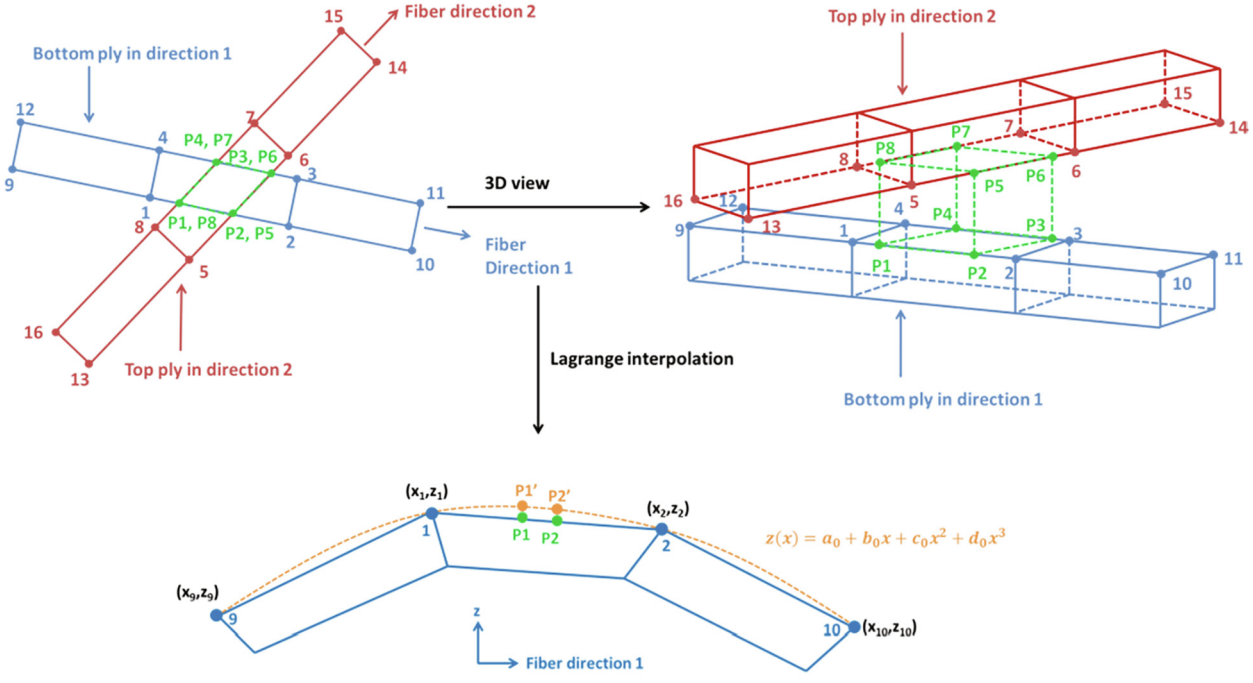

Fig. 15. Third configuration for curvature calculation: Lagrange interpolation.

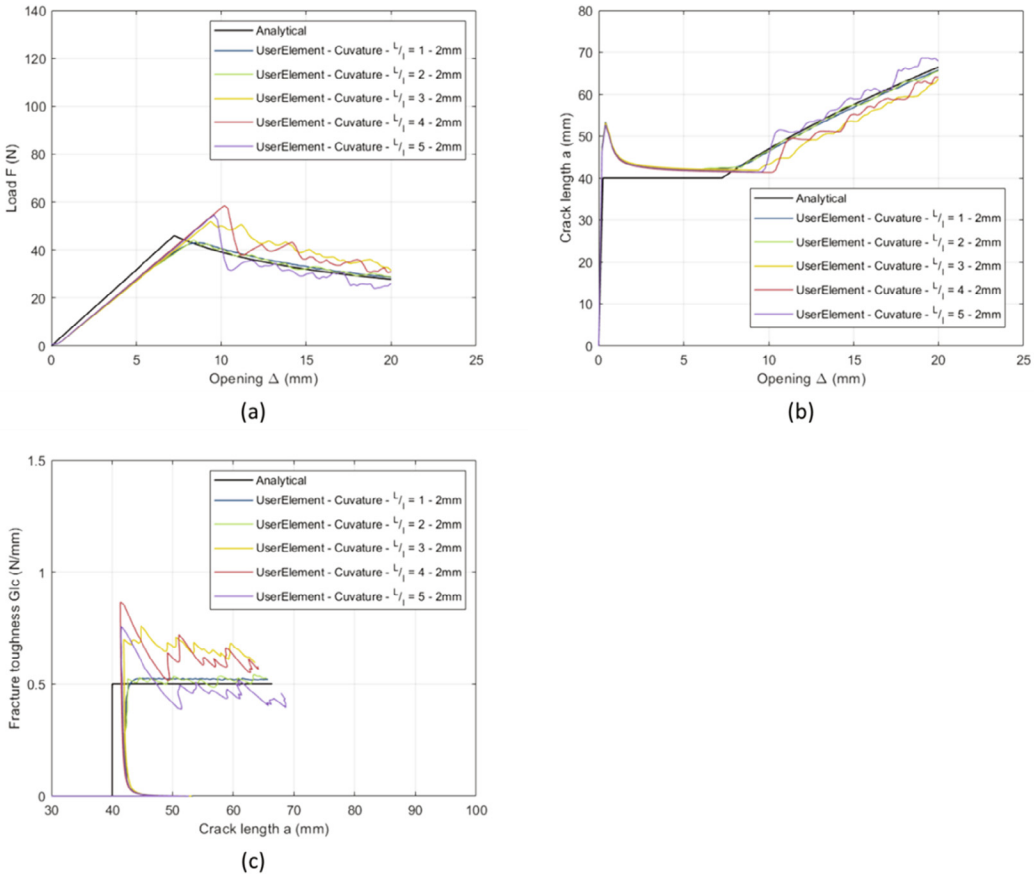

Fig. 16. Force/displacement curves (a), crack length/opening displacement curves and fracture toughness/crack length curves (c) for different mesh configurations of a 2 mm thick laminate with bending curvature consideration.

tual nodes on the edge 1–2 (P'_1 and P'_2) is obtained in solving the cubic function passing through real nodes 9, 1, 2 and 10, nodes 9 and 10 being upper nodes of the two neighboring elements of the bottom ply (Fig. 14). Coordinates of those nodes allow to evaluate the constants a_0, b_0, c_0 and d_0. Results obtained with this new bending curvature consideration are presented in the following part.

So, finally, this interface element is an eight virtual nodes interface element (P'_1 and P'_8) implemented in a 16-node user element (Fig. 15) using an Abaqus/Explicit VUEL subroutine. These sixteen nodes are the four upper nodes of the bottom ply element (1, 2, 3 and 4 in blue) plus the two other upper nodes of the two neighboring elements (9, 12 and 10, 11), and the four lower nodes of the top ply element (5, 6, 7 and 8 in red) plus the two other lower nodes of the two neighboring elements (13, 16 and 14, 15).

$$z(x) = \sum_{j=9,1,2,10} z_j \left(\prod_{\substack{i=9,1,2,10 \\ i \neq j}} \frac{x - x_i}{x_j - x_i} \right) \tag{9}$$

5. Results in fracture mode I and II with the bending curvature consideration

5.1. Fracture mode I

Different mesh configurations (Fig. 8) are simulated taking into account the bending curvature in fracture mode I for both 2 mm and 4 mm thick specimens. Force/opening displacement curves, crack length/opening displacement curves and fracture toughness/crack length curves are presented in Fig. 16 for 2 mm thick laminate and in Fig. 17 for 4 mm thick laminate. For both cases the implementation of the bending curvature consideration makes it possible to get a good correlation between analytical and numerical results for all element length to width ratios. Curves plotted in Fig. 18 summarize these results by comparing the error in the average value of the fracture toughness G_{IC} for each specimen and length to width ratio. The improvement is logically more important for the thin specimen but nerveless the error in G_{IC} is also decreased for the thick specimen. For the two specimens, and with the bending curvature consideration, the maximum error is close to 30% for $\frac{L}{l} = 3$ and $\frac{L}{l} = 4$. For $\frac{L}{l} = 5$ the comparison between analytical and numerical results is almost perfect even if the curvature seems a little overestimated with a crack length growth slightly ahead (Figs. 16-b and 17-b).

Finally these results are confirmed with the Fig. 19, showing the comparison between the deformed shape of the reference case, in black ($\frac{L}{l} = 1$), and a case with bending curvature consideration ($\frac{L}{l} = 5$), in blue, for an opening displacement of 20 mm. As already highlighted for the ratio length to width of five, the crack length growth is in advance of 3.5 mm compared to the reference. This is better than the delay of 9 mm observed without considering the bending curvature (Fig. 12). The effect of the bending curvature consideration is also visible in the deformed shape. Even when the element size is increased, the bending is well represented. According to these results the new interface element can be validated in fracture mode II.

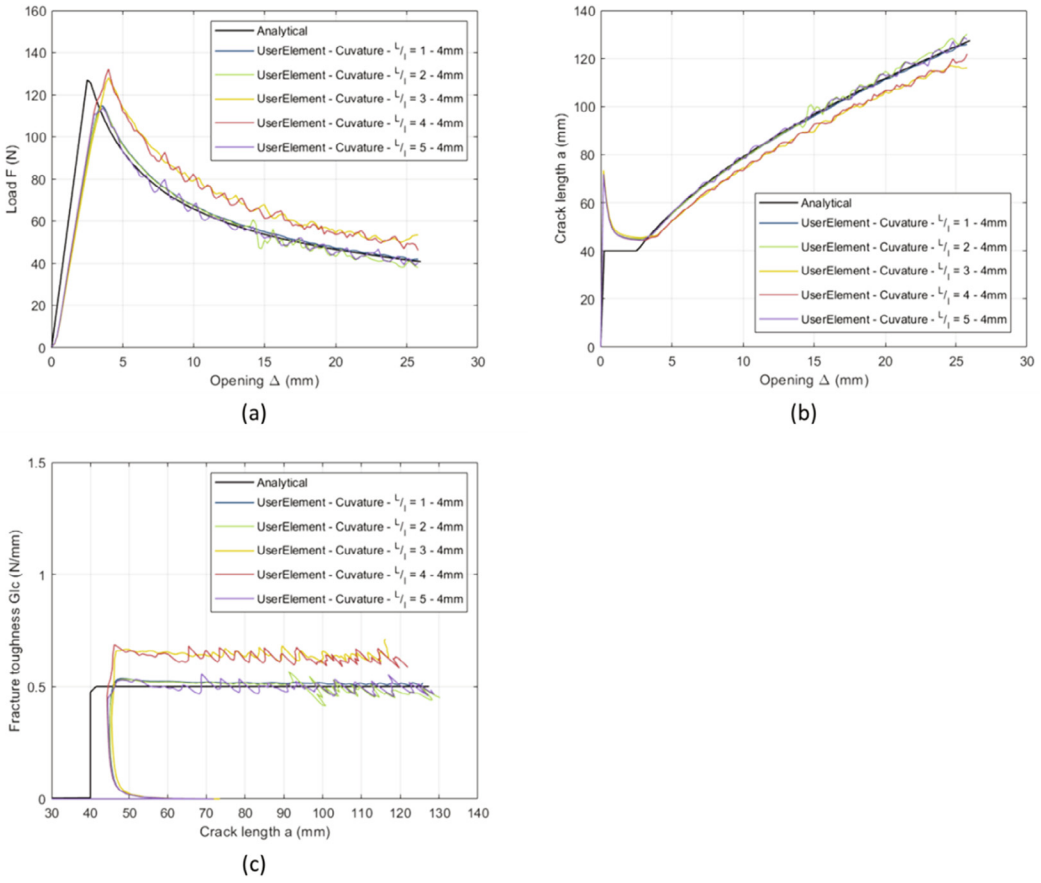

Fig. 17. Force/displacement curves (a), crack length/opening displacement curves and fracture toughness/crack length curves (c) for different mesh configurations of a 4 mm thick laminate with bending curvature consideration.

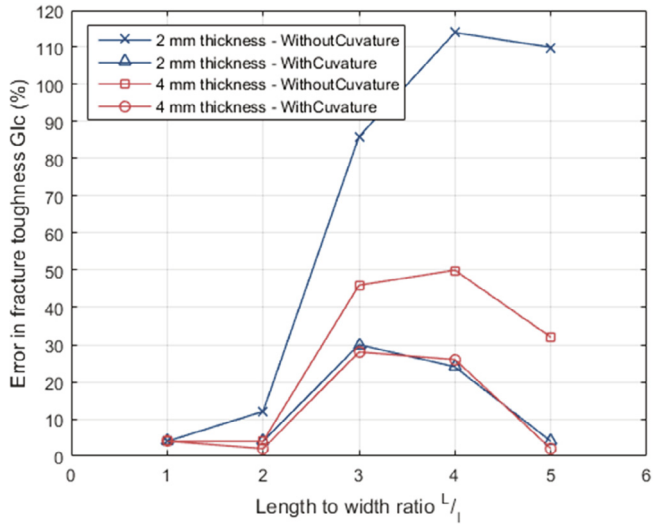

Fig. 18. Error in fracture toughness in mode I according to element length to width ratio for 2 and 4 mm thick specimens.

5.2. Fracture mode II

In order to validate the new interface element in delamination mode II, an "End Notched Flexure" (ENF) test is simulated. Both 2 mm and 4 mm thick laminates presented in Section 3 are tested. The test is shown in Fig. 20. Concerning the specimen, the only difference is the pre-crack size which is set to 60 mm to get a stable delamination. Indeed the stability condition of the crack growth is reached for $a_0 > 0.347L$ [48]. The ENF test is more stable than the DCB test. Moreover, the bending curvature consideration is much less significant for fracture shearing mode because the in-plane stiffness of the arms of the ENF tests is much more important than their out-of-plane stiffness. In this way the bending curvature correction implemented for the delamination mode I is not taken into account in the mode II opening calculation.

Different mesh configurations are simulated as presented in Section 3 (Fig. 8). Numerical force/opening displacement curves are compared to the analytical solution (Fig. 21). The analytical curve is obtained with the analysis method given by the fracture mode II test standard [45] and detailed in [48]. A good correlation between numerical and analytical results is observed for each mesh configuration and for both specimens. As in mode I, results are very similar for $\frac{L}{l} = 5$, and the load is a little overestimated for $\frac{L}{l} = 3$ and $\frac{L}{l} = 4$. According to these results, the new interface element is also validated in fracture mode II.

5.3. Computation time

Another objective of the implementation of this new delamination element in the DPM is to decrease computation time. The new interface element gives the possibility to increase ply volume element length in the fiber orientation, which allows to reduce the number of elements and then to lighten the model. Simulations run to write this paper were launched with 36 CPUs on the high performance calculator CALMIP [https://www.calmip.univ-toulouse.fr]. Fig. 22 pre-

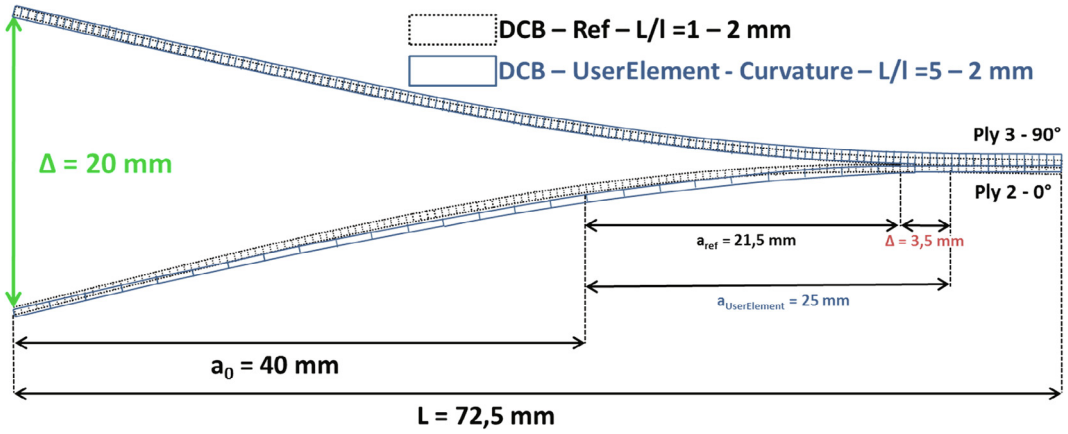

Fig. 19. Better bending curvature consideration (for a deformation scale factor of 10). Only ply 2 and ply 3 are depicted.

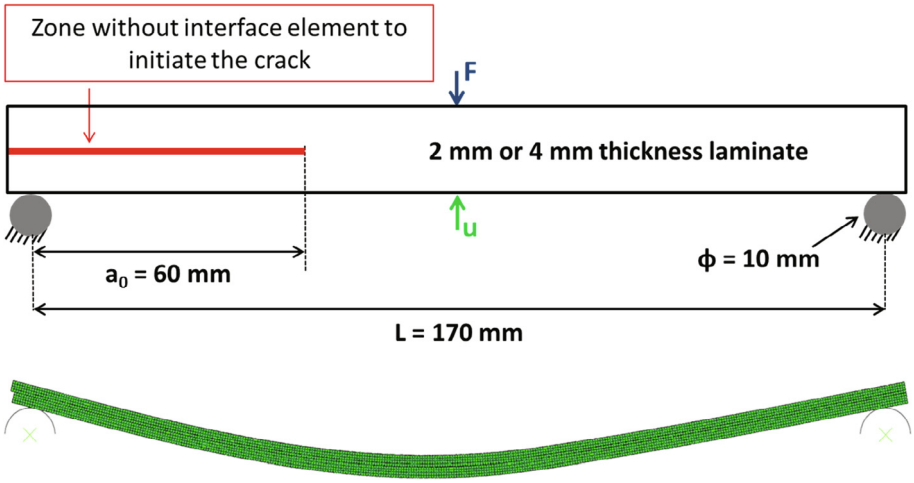

Fig. 20. ENF test.

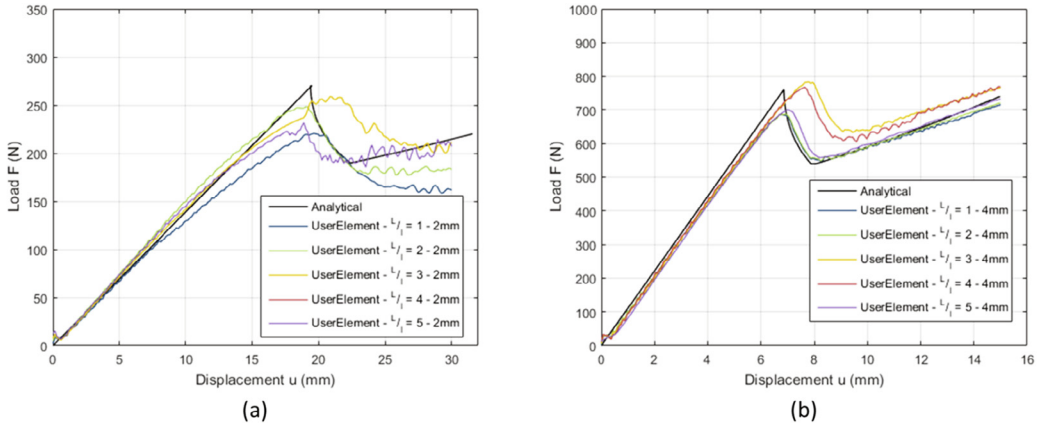

Fig. 21. Force/opening displacement curves in mode II (a), 2 mm thick laminate and (b), 4 mm thick laminate.

sents the evolution of computation time according to the mesh configuration for mode I and mode II tests. As expected, an important decrease of calculation time is observed. Indeed computation time is divided by 3.5 for the DCB simulation and by 4.4 for the ENF simulation when the length to width ratio increases from one to five. The new interface element implementation is efficient to lighten the DPM.

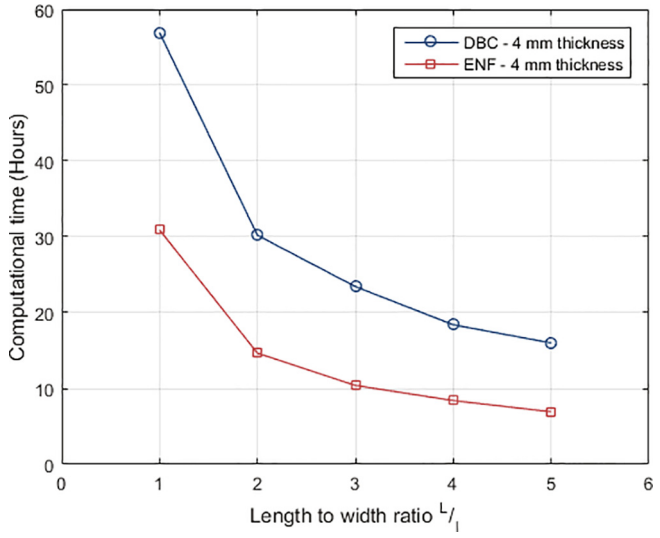

Fig. 22. Computational time according to element length to width ratio for DCB and ENF tests.

6. Conclusion

In this paper a user element to simulate delamination in composite laminate with non-coincident ply meshes was developed in order to be implemented in the Discrete Ply Model in Abaqus /Explicit. It is a classical interface element inside a 16-node user element, computed from eight virtual nodes corresponding to the intersection of ply volumes elements edges. First DCB test simulations for a thin laminate (2 mm-thickness) and a thick laminate (4 mm-thickness) with various element length to width ratios have shown non-concluding results for ratios superior to two. Above, differences on the crack propagation initiation were observed. The issue was identified as a poor curvature consideration in interface elements when loaded in bending. Indeed increasing volume element length in the fiber orientation degrades bending model discretization. To solve this problem, a bending curvature consideration was implemented in the user element. Taking into account this curvature allows to get a better convergence of the model in mode I. The new element was also tested and validated in fracture mode II through ENF tests.

Thus, this study has shown that it is possible, thanks to this new user interface element, to model plies using volume elements with a high length to width ratio and with non-coincident nodes to simulate the delamination in 0°/90° or 90°/0° interfaces of composite laminates. It gives acceptable results for engineering problems, given the fact that one of the consequences of volume element length increase enabled by this new interface is the computation time reduction by 3.5 for the DCB test and by 4.4 for the ENF test, which is an important point to make the model usable in the industry.

This work only focuses on 8-node interface elements made by 4 sides overlapping zone (colored in green in Fig. 3) but should be generalized to the other unclassical case; this work is in progress. The next step of this work is to validate the new interface element for other fiber orientations as for example 45°/-45° and in complex application cases such as simulation of delamination due to out-of-plane impact on laminates.

CRediT authorship contribution statement

A. Trellu: Conceptualization, Methodology, Validation, Formal analysis, Investigation, Data curation, Writing - original draft. **C. Bouvet:** Conceptualization, Methodology, Software, Validation, Formal analysis, Investigation, Resources, Data curation, Writing - original draft, Writing - review & editing, Supervision, Project administration, Funding acquisition. **S. Rivallant:** Conceptualization, Methodology, Software, Validation, Formal analysis, Investigation, Resources, Data curation, Writing - original draft, Writing - review & editing, Supervision. **L. Ratsifandrihana:** Methodology, Validation, Formal analysis, Investigation, Resources, Supervision, Project administration, Funding acquisition.

Declaration of Competing Interest

The authors declare that they have no known competing financial interests or personal relationships that could have appeared to influence the work reported in this paper.

Acknowledgments

Authors would like to gratefully acknowledge CALMIP (CALcul en Midi-Pyrénées, (https://www.calmip.univ-toulouse.fr) for access to the HPC resources under the allocation p1026.

References

[1] Morteau E, Fualdes C. Composites @ Airbus, Damage Tolerance Methodology. FAA Workshop for Composite Damage Tolerance and Maintenance, Chicago IL; 2006.
[2] Abrate S. Impact on composite structures. Cambridge University Press; 1998.
[3] Reid SR, Zhou G. Impact behaviour of fibre-reinforced composite materials and structures. Cambridge, England: Woodhead Publishing, Elsevier; 2016.
[4] Wisnom MR. Modelling discrete failures in composites with interface elements. Compos A Appl Sci Manuf 2010;41(7):795–805.
[5] Yang QD, Cox BN, Fang XJ, Zhou ZQ. Virtual testing for advanced aerospace composites: advances and future needs. J Eng Mater Technol 2011;133(1):011002.
[6] Eve O. Etude du comportement des structures composites endommagées par impact basse vitesse PhD Thesis. France: University of Metz; 1999.
[7] Richardson MOW, Wisheart MJ. Review of low-velocity impact properties of composite materials. Compos A Appl Sci Manuf 1996;27(12):1123–31.
[8] Bouvet C, Castanié B, Bizeul M, Barrau JJ. Low velocity impact modeling in laminate composite panels with discrete interface elements. Int J Solids Struct 2009;46(14–15):2809–21.
[9] Bouvet C, Rivallant S, Barrau JJ. Low velocity impact modeling in composite laminates capturing permanent indentation. Compos Sci Technol 2012;72:1977–88.
[10] Rivallant S, Bouvet C, Hongkarnjanakul N. Failure analysis of CFRP laminates subjected to compression after impact : FE simulation using discrete interface elements. Compos A Appl Sci Manuf 2013;55:83–93.
[11] Serra J, Bouvet C, Castanié B, Petiot C. Experimental and numerical analysis of Carbon Fiber Reinforced Polymer notched coupons under tensile loading. Compos Struct 2017;181:147–57.
[12] Dubary N, Bouvet C, Rivallant S, Ratsifandrihana L. Damage tolerance of an impacted composite laminate. Compos Struct 2018;206:261–71.
[13] Abaqus 2016 Analysis user's manual, Dassault Systemes Simulia; 2016
[14] Lopes CS, Sadaba S, Gonzalez C, J. LLorca, pp. Camanho. Physically-sound simulation of low-velocity impact on fiber reinforced laminates. Int J Impact Eng 2016;92:3–17.
[15] Waas AM, Joseph APK, Davidson P. Open Hole and filled hole progressive damage and failure analysis of composite laminates with a countersunk hole. Composites Structures 2018;203:523–38.
[16] Falcó O, Ávila RL, Tijs B, Lopes CS. Modelling and simulation methodology for unidirectional composite laminates in a Virtual Test Lab framework. Compos Struct 2018;190:137–59.
[17] Liu S, Kutlu Z, Chang F. Matrix cracking-induced delamination propagation in graphite/epoxy laminated composites due to transverse concentrated load. Compos Mater: Fatigue Fract 1993;4:86–101.
[18] Lammerant L. Modelling of the interaction between matrix cracks and delaminations during impact of composite plates. Compos Sci Technol 1996;56 (10):1171–8.
[19] de Moura MFSF, Gonçalves JPM. Modelling the interaction between matrix cracking and delamination in carbon–epoxy laminates under low velocity impact. Compos Sci Technol 2004;64:1021–7.
[20] Hallett SR, Jiang WG, Khan B, Wisnom MR. Modelling the interaction between matrix cracks and delamination damage in scaled quasi-isotropic specimens. Compos Sci Technol 2008;68(1):80–9.
[21] Maimi P, Rodriguez H, Blanco N, Mayugo JA. Numerical modeling of matrix cracking and intralaminar failure in advanced composite materials. In Numerical Modelling of Failure in Advanced Composite Materials, Edited by P.P.Camanho, S. R.Hallett, Woodhead Publishing Series in Composites Science and Engineering: Number 62; 2015.
[22] Leopold C, Harder S, Buggish C, Leibig WV, Fiedler B. Influence of 90° layer thickness on damage initiation and propagation in CFRP cross ply laminates. In: 17th European conference on composite materials, Allemagne; 2016

[23] Bazant ZP, Oh BH. Crack band theory for fracture of concrete. Matér Constr 1983;16(3):155–77.
[24] Krueger R. The virtual crack closure technique: history, approach and applications. NASA/Contractor Report-2002-211628; 2002
[25] Dugdale DS. Yielding of steel sheets containing slits. J. Mech. Phys. Solids 1960;8:100–8.
[26] Barenblatt GI. The mathematical theory of equilibrium of cracks in brittle fracture. Adv. Appl. Mech. 1962;7:55–129.
[27] Harper P, Hallet SR. Cohesive zone length in numerical simulations of composite delamination. Eng Fract Mech 2008;75(16):4774–92.
[28] Dongen BV, Oostrum AV, Zarouchas D. A blended continuum damage and fracture mechanics method for progressive damage analysis of composite structures using XFEM. Compos Struct 2018;184:512–22.
[29] Turon A, Dávila CG, Camanho PP, Costa J. An engineering solution for mesh size effects in the simulation of delamination using cohesive zone models. Eng Fract Mech 2007;74(10):1665–82.
[30] Aymerich F, Dore F, Priolo P. Prediction of impact-induced delamination in cross-ply composite laminates using cohesive interface elements. Compos Sci Technol 2008;68:2383–90.
[31] Alfano G, Crisfield MA. Finite element interface models for the delamination analysis of laminated composites: mechanical and computational issues. Int. J. Numer. Meth. Engng 2001;50:1701–36.
[32] Allix O, Ladevèze P. Interlaminar interface modelling for the prediction of delamination. Compos Struct 1992;22:235–42.
[33] Gens A, Carol I, Alonso EE. An interface element formulation for the analysis of soil-reinforcement interaction. Comput Geotech 1988;7:133–51.
[34] Camanho PP, Davila CG, De Moura MF. Numerical simulation of mixed-mode progressive delamination. J Compos Mater 2003;37(16):1415–38.
[35] Tvergaard V, Hutchinson JW. The relation between crack growth resistance and fracture process parameter in elastic-plastic solids. J Mech Phys Solids 1992;40 (6):1377–97.
[36] Jensen SM, Martos MJ, Bak BLV, Lindgaard E. Formulation of a mixed-mode multilinear cohesive zone law in an interface finite element for modelling delamination with R-curve effects. Compos Struct 2019;216:477–86.
[37] Dávila CG, Camanho PP, Turon A. Cohesive Elements for Shells. NASA/TP-2007-214869; 2007.
[38] Kohnehpooshi O, Noorzaei J, Jaafar MS, Raizal Saifulnaz MR. Development of a special interface element between brick and plate bending elements. Procedia Eng 2011;14:734–42.
[39] Navarro P, Pascal F, Aubry J, Marguet S, Ferrero JF, Lemaire S, et al. Semi-continuous approach for the study of impacts on woven composite laminates: Modeling interlaminar behavior with a specific interface element. Int J Impact Eng 2015;75:184–93.
[40] Tawk I, Navarro P, Ferrero J-F, Barrau J-J, Abdullah E. Composite delamination modelling using a multi-layered solid element. Compos Sci Technol 2010;70 (2):207–14.
[41] Shor O, Vaziri R. Application of the local cohesive zone method to numerical simulation of composite structures under impact loading. Int J Impact Eng 2017;104:127–49.
[42] Belytschko T, Krongauz Y, Organ D, Fleming M, Krysl P. Meshless methods: an overview and recent developments. Comput Methods Appl Mech Eng 1996;139 (1–4):3–47.
[43] Funari MF, Lonetti P, Spadea S. A crack growth strategy based on moving mesh method and fracture mechanics. Theor Appl Fract Mech 2019;102:103–15.
[44] ASTM D5228 - Standard test method for mode I interlaminar fracture toughness of unidirectional fiber-reinforced polymer matrix composites. Rapport technique; 2001
[45] ASTM D7905 - Standard test method for determination of the Mode II interlaminar fracture toughness of unidirectional fiber-reinforced polymer matrix composites. Rapport technique; 2014
[46] Wilson EL, Taylor RL, Doherty WP, Ghaboussi J. Incompatible displacement models. numerical and computer methods in structural mechanics. Academic Press; 1973. p. 43–57.
[47] Batoz JL, Dhatt G. Modélisation des structures par éléments finis. Hermès-Lavoisier; 1990
[48] Bouvet C. Fracture mechanics of composite: delamination and cracking. Techniques de l'Ingénieur, TRP4043 V1; 2019